SCIENCE CHINA
Physics, Mechanics & Astronomy

• Article •

March 2014 Vol. 57 No. 3: 555–561
doi: 10.1007/s11433-014-5396-2

Floquet analysis of fundamental, subharmonic and detuned secondary instabilities of Görtler vortices†

REN Jie & FU Song*

School of Aerospace Engineering, Tsinghua University, Beijing 100084, China

Received July 15, 2013; accepted September 27, 2013; published online January 23, 2014

Nonlinear parabolized stability equations are employed in this work to investigate the nonlinear development of the Görtler instability up to the saturation stage. The perturbed boundary layer is highly inflectional both in the normalwise and spanwise directions and receptive to the secondary instabilities. The Floquet theory is applied to solve the fundamental, subharmonic and detuned secondary instabilities. With the Görtler-vortices-distorted base flow, two classes of secondary disturbances, i.e. odd modes and even modes, are identified according to the eigenfunctions of the disturbances. These modes may result in different patterns in the late stages of the transition process. Li and Malik [1] have shown the sinuous and varicose types of breakdown originating from the odd and even modes. The current study focuses on the four most amplified modes termed the even modes I & II and odd modes I & II. Odd mode II was missing in the work of Li and Malik [1] probably due to their inviscid simplification. The detuned modes are confirmed to be less amplified than the fundamental (for the odd mode I) and subharmonic modes (for even modes I & II and the odd mode II).

Görtler vortices, secondary instability, Floquet theory

PACS number(s): 47.20.Lz, 47.20.Qr

Citation: Ren J, Fu S. Floquet analysis of fundamental, subharmonic and detuned secondary instabilities of Görtler vortices. Sci China-Phys Mech Astron, 2014, 57: 555–561, doi: 10.1007/s11433-014-5396-2

1 Introduction

The boundary layer centrifugal instability excited by the surface roughness or the free-stream turbulence [2] along a concave wall is commonly known as the Görtler instability. As a result of the sustained imbalance between the centrifugal force and the normal pressure gradient, the streamwise counter-rotating longitudinal vortices with a quasi-constant spanwise wavelength are produced. The steady streamwise vortices give rise to highly distorted profiles both in the normal and spanwise directions which are receptive to the high-frequency secondary instabilities. Complete reviews on the Görtler instabilities are given by Herbert [3], Hall [4], Floryan [5] and Saric [6].

The Görtler vortices as such are not the indicators of the transition-onset. The main reason for the breakdown is the high frequency secondary instabilities of the vortices. Herbert's [7] secondary instability theory (Floquet theory) well explained the subharmonic type mode of the plane Poiseuille flows. The application of the Floquet theory in the secondary instabilities has been reviewed by Herbert [8] in detail.

As one of the most comprehensive experiments, Swearingen and Blackwelder [9] studied the growth and breakdown of the Görtler vortices using hot-wire rakes. In their experiment, nothing was done to fix the spanwise wavelength, i.e. naturally developed vortices were given birth and the vortices triggered inviscid shear layer instabilities. Both the horseshoe vortex structure and the sinuous oscillations were observed in the late stage of the transition process.

*Corresponding author (email: fs-dem@tsinghua.edu.cn)

†Contributed by FU Song (Associate Editor-in-Chief)

With the successful observation and measurement of the experiment [9], several numerical studies have been carried out aiming at the nonlinear development of the Görtler vortices and their secondary instability. Lee and Liu [10] obtained the mushrooms with a finite-difference method. The streamwise velocity matches well the experiment [9] before the secondary disturbances set in. The development of the Görtler instability can be reasonably characterized with the marching method (e.g. the parabolized stability equations). The application of the nonlinear parabolized stability equations (NPSE) in the simulation of the Görtler instability goes back to Hall [11]. The inflectional profiles of the streamwise velocity were demonstrated and as a result the Rayleigh-type secondary instabilities were anticipated. Studies of the secondary instability were given in a following paper by Hall and Horseman [12]. The odd and the even modes which correspond to the experimental observations [9] were obtained. NPSE, as applied to the streamwise vortices, belongs to an ad hoc simplification as the streamwise wavenumber $\alpha \equiv 0$. Hence, the iteration on the wavenumber is not applied. The NPSE has been successfully used in the spatial growth of disturbances including the 2D TS modes, 3D oblique modes, crossflow vortices and the Görtler instabilities. For a detailed review of this method, the reader may refer to Herbert [13].

Li and Malik [1] investigated the secondary instability including both the fundamental and the subharmonic types. The influence of the wavelength on the odd (dominating at small wavelengths and resulting in sinuous-type break down) and the even (dominating at large wavelengths and resulting in varicose-type break down) modes are clarified. Subharmonics of both the odd and even modes were observed to have comparable growth rates to their fundamental counterparts. Yu and Liu [14] verified the growth rate obtained from the secondary instability with the global energy balance method and showed that sinuous mode will dominate.

The effect of curvature variation has been considered by Benmalek and Saric [15] using NPSE. A stabilization effect was confirmed for the Görtler vortices which developed from a concave surface into a flat or convex section. The secondary instability was thus suppressed as the inflection profiles vanished. Also with the PSE approach, Cunff and Zebib [16] studied the Görtler vortices in the wall jet flow and captured the primary instability in the experiment. Liu et al. [17] studied the secondary instability of boundary layer distorted with both Klebanoff streaks and the Tollmien-Schlichting waves. The results of the Floquet analysis show that the interaction of the steaks and the TS waves can result in different manners depending on the wave number and the amplitude of the streaks.

More recently, Wu et al. [18] formulated the initial-boundary-value problem accounting for the receptivity and the development of the induced disturbances. The asymptotic analysis showed the distinct regimes where a fixed wavelength disturbance would evolve. Schrader et al. [19] studied the receptivity, instability and breakdown of the Görtler vortices with spatial DNS (Direct Numerical Simulation). Xu el al. studied the secondary instability of crossflow vortices with both incompressible [20] and compressible [21] formulations showing that wall suction can effectively suppress the crossflow instability as well as its secondary instability.

However, most of the secondary instability studies fell into the scope of the inviscid analysis with a resulting simplified stability equation. The inviscid assumptions cannot give the real physics of the disturbances in the high-shear region. The present study is carried out under the experiment of Swearingen and Blackwelder [9]. The viscous and compressible Floquet system is established and the fundamental, subharmonic and detuned secondary instabilities are studied. In sect. 2, the formulation of the NPSE is given and the base flow is obtained. Sect. 3 formulates the Floquet system and the related numerical method is introduced. The results of the fundamental mode are given in sect. 4. The influences of the Floquet parameter, i.e. the detuned and subharmonic on the secondary instabilities are clarified in sect. 5 followed by the concluding remarks in sect. 6.

2 NPSE and the saturated Görtler vortices

Following Chang and Malik [22], the disturbance equations for the density, velocities and temperature, i.e., $\tilde{q} = \left(\tilde{\rho}, \tilde{u}, \tilde{v}, \tilde{w}, \tilde{T}\right)$ can be represented below in a compact form.

$$\begin{aligned}\boldsymbol{\Gamma}\frac{\partial \tilde{q}}{\partial t} + \boldsymbol{A}\frac{\partial \tilde{q}}{\partial x} + \boldsymbol{B}\frac{\partial \tilde{q}}{\partial y} + \boldsymbol{C}\frac{\partial \tilde{q}}{\partial z} + \boldsymbol{D}\tilde{q} \\ = \boldsymbol{H}_{xx}\frac{\partial^2 \tilde{q}}{\partial x^2} + \boldsymbol{H}_{xy}\frac{\partial^2 \tilde{q}}{\partial x \partial y} \\ + \boldsymbol{H}_{xz}\frac{\partial^2 \tilde{q}}{\partial x z} + \boldsymbol{H}_{yy}\frac{\partial^2 \tilde{q}}{\partial y^2} + \boldsymbol{H}_{yz}\frac{\partial^2 \tilde{q}}{\partial y \partial z} + \boldsymbol{H}_{zz}\frac{\partial^2 \tilde{q}}{\partial z^2} + N. \quad (1)\end{aligned}$$

Matrices (5×5) $\boldsymbol{\Gamma}$, $\boldsymbol{A}$, $\boldsymbol{B}$, $\boldsymbol{C}$, $\boldsymbol{D}$, $\boldsymbol{H}_{xx}$, $\boldsymbol{H}_{yy}$, $\boldsymbol{H}_{zz}$, $\boldsymbol{H}_{xy}$, $\boldsymbol{H}_{yz}$ and $\boldsymbol{H}_{xz}$ represent the coefficients that are functions of the *Re*, *Ma*, *Pr* numbers, curvature and base flow quantities. These matrices can be found in ref. [21]. The *Pr* number is assumed to be 0.72 in the flow. Stokes's hypothesis and the Sutherland law are employed for the closure of the disturbance equations. The streamwise, normalwise and spanwise coordinates are denoted with *x*, *y* and *z* respectively. In the frame work of the NPSE, the disturbances and the nonlinear terms are expressed by the truncated Fourier series, i,e.

$$\begin{aligned}&\tilde{q}(x, y, z, t) \\ &= \sum_{m=-M}^{M}\sum_{n=-N}^{N} \hat{\varphi}_{mn}(x, y) \exp\left(\mathrm{i}\int \alpha_{mn}(x)\,\mathrm{d}x + \mathrm{i}n\beta z - \mathrm{i}m\omega t\right), \quad (2)\end{aligned}$$

$$N = \sum_{m=-M}^{M}\sum_{n=-N}^{N} \hat{f}_{mn} \exp(\mathrm{i}n\beta z - \mathrm{i}m\omega t). \quad (3)$$

Here α is the streamwise wavenumber which is identical to zero. The spanwise wavenumber and the disturbance frequency are denoted with β and ω respectively. It should be

noted that $\omega = 0$ corresponds to the steady vortices. By substituting the series (2) and (3) into the stability equation (1), the shape functions of the Fourier mode (m, n) is thus governed by

$$\begin{aligned}\boldsymbol{H}_x\frac{\partial\hat{\varphi}_{mn}}{\partial x} + \boldsymbol{H}_y\frac{\partial\hat{\varphi}_{mn}}{\partial y} + \boldsymbol{H}\hat{\varphi}_{mn} &= \boldsymbol{H}_{xx}\frac{\partial^2\hat{\varphi}_{mn}}{\partial x^2} + \boldsymbol{H}_{xy}\frac{\partial^2\hat{\varphi}_{mn}}{\partial x\partial y} + \boldsymbol{H}_{yy}\frac{\partial^2\hat{\varphi}_{mn}}{\partial y^2} \\ &\quad + \hat{F}_{mn}\exp\left(-\mathrm{i}\int\alpha_{mn}\mathrm{d}x\right),\end{aligned} \tag{4}$$

where $\hat{\varphi} = \left(\hat{\rho}, \hat{u}, \hat{v}, \hat{w}, \hat{T}\right)$ and the matrices $\boldsymbol{H}_x$, $\boldsymbol{H}_y$ and $\boldsymbol{H}$ are given by

$$\boldsymbol{H}_x = \boldsymbol{A} - 2\mathrm{i}\mathbf{H}_{xx}\alpha_{mn} - \mathrm{i}n\beta\mathbf{H}_{xz}, \tag{5a}$$

$$\boldsymbol{H}_y = \boldsymbol{B} - \mathrm{i}\mathbf{H}_{xy}\alpha_{mn} - \mathrm{i}n\beta\mathbf{H}_{yz}, \tag{5b}$$

$$\begin{aligned}\boldsymbol{H} = {} & \boldsymbol{D} - \mathrm{i}m\omega\boldsymbol{\Gamma} + \mathrm{i}n\beta\boldsymbol{C} + \beta^2n^2\mathbf{H}_{zz} + \mathrm{i}\alpha_{mn}\boldsymbol{A} \\ & + \left({\alpha_{mn}}^2 - \mathrm{i}\frac{\partial\alpha_{mn}}{\partial x}\right)\boldsymbol{H}_{xx} + n\beta\alpha_{mn}\boldsymbol{H}_{xz}.\end{aligned} \tag{5c}$$

Notice that $\alpha \equiv 0$ and

$$\frac{\partial}{\partial x} \sim O\left(\frac{1}{Re}\right), \quad \boldsymbol{H}_{xx} \sim \boldsymbol{H}_{xy} \sim \boldsymbol{H}_{yy} \sim O\left(\frac{1}{Re}\right). \tag{6}$$

The analysis of the order of magnitude (6) enables the parabolization of the governing equations of the shape function (4) into PSE, i.e,

$$\boldsymbol{H}_x\frac{\partial\hat{\varphi}_{mn}}{\partial x} + \boldsymbol{H}_y\frac{\partial\hat{\varphi}_{mn}}{\partial y} + \boldsymbol{H}\hat{\varphi}_{mn} = \boldsymbol{H}_{yy}\frac{\partial^2\hat{\varphi}_{mn}}{\partial y^2} + \hat{F}_{mn}. \tag{7}$$

The Fourier modes (m, n) are calculated with the Dirichlet boundary conditions. For the $(0, 0)$ mode, we apply the Neumann condition at the far field to the normal velocity to assure mass conservation:

$$\begin{aligned}&\hat{u}_{mn} = \hat{v}_{mn} = \hat{w}_{mn} = \hat{T}_{mn} = 0, \quad y = 0, \\ &\hat{u}_{mn} = \hat{v}_{mn} = \hat{w}_{mn} = \hat{T}_{mn} = 0, \quad y \to \infty, \\ &\hat{u}_{00} = \frac{\partial\hat{v}_{00}}{\partial y} = \hat{w}_{00} = \hat{T}_{00} = 0, \quad y \to \infty.\end{aligned} \tag{8}$$

The parabolized equations (7) now can be solved with a marching procedure in the x direction. Following Schmid and Henningson [23], to achieve the highest possible accuracy, we apply the mapping

$$y = a\frac{1+\bar{y}}{b-\bar{y}}, \; a = \frac{y_i y_{\max}}{y_{\max} - 2y_i}, \; b = 1 + \frac{2a}{y_{\max}}, \; \bar{y} \in [-1, 1] \tag{9}$$

in the normal wise direction, which allows for a clustering of one half of the grid points to the interval $[0, y_i]$ accompanied by the fourth-order central difference scheme

$$\frac{\partial\hat{\varphi}_j}{\partial y} = \frac{\hat{\varphi}_{j-2} - 8\hat{\varphi}_{j-1} + 8\hat{\varphi}_{j+1} - \hat{\varphi}_{j+2}}{12\Delta y}, \tag{10a}$$

$$\frac{\partial^2\hat{\varphi}_j}{\partial y^2} = \frac{-\hat{\varphi}_{j-2} + 16\hat{\varphi}_{j-1} - 30\hat{\varphi}_j + 16\hat{\varphi}_{j+1} - \hat{\varphi}_{j+2}}{12(\Delta y)^2}. \tag{10b}$$

The marching is proceeded with an implicit Euler scheme and the nonlinear terms are iterated until the residual is less than the prescribed tolerance, e.g. 10^{-10}. The base flow is calculated until the saturation state of the Görtler vortices in accordance with the experiment [9] is reached.

The cases shown below follow the NPSE calculations of Li and Malik [1] where the parameters are taken from the experiment of Swearingen and Blackwelder [9]. The freestream velocity is 5 m/s and the radius of curvature of the concave surface is 3.2 m. The marching procedure is applied within 0.1 m $\leqslant x \leqslant$ 1.4 m. The initial shape of the disturbances is given by the normal mode analysis and the specified amplitude is $u = 0.0187U_\infty$ on the basis of the experiment. In the category of the incompressible flows, the energy of a particular Fourier component is defined as

$$E_{(0,n)} = \int_0^\infty |\hat{u}_{0n}|^2 + |\hat{v}_{0n}|^2 + |\hat{w}_{0n}|^2\mathrm{d}y, \quad n \neq 0, \tag{11a}$$

$$E_{(0,0)} = \int_0^\infty |\hat{u}_{00}|^2 + |\hat{w}_{00}|^2\mathrm{d}y. \tag{11b}$$

The nonlinear development of the Görtler vortices demonstrated by the disturbance energy is shown in Figure 1. The spanwise wavelength λ is 0.009, 0.018 and 0.036 m respectively and the comparison with Li and Malik [1] is made for the case of 0.009 m wavelength. The disturbance energy matches Li and Malik well. A global watch of the nonlinear development of the Görtler vortices is shown in Figure 2. Ten slices of the streamwise velocity are given ranging from $x = 0.1$ m to $x = 1.2$ m.

The steady streamwise Görtler vortices distorted the Blasius boundary layer in the normalwise and spanwise directions and resulted in highly inflectional profiles. The gradients of the streamwise velocity are shown in Figures 3 and 4. for the 18 mm case.

The flow field with the saturated Görtler vortices will be used as the base flow of the subsequent secondary instabilities.

3 Formulation of the Floquet system

In the methodology of the Floquet theory, the secondary disturbances are expressed as

$$\tilde{q}_s(x, y, z, t) = \mathrm{e}^{\gamma z}\mathrm{e}^{\sigma t + \mathrm{i}\alpha_s x}\sum_{m=-\infty}^{\infty}\hat{q}_m(y)\,\mathrm{e}^{\mathrm{i}m\beta z}, \quad 0 \leqslant \gamma_i \leqslant \frac{\beta}{2}. \tag{12}$$

Here $\gamma_i = 0$ gives the fundamental secondary instability while $\gamma_i = 0.5\beta$ results in the subharmonic modes. The remaining choices of γ_i produce the detuned modes. The parameter α_s is the streamwise wavenumber of the secondary disturbances. The present study focuses on the temporal evolution of the disturbances and thus α_s is prescribed and σ is the eigenvalue to determine. By ignoring the variation of the base flow in

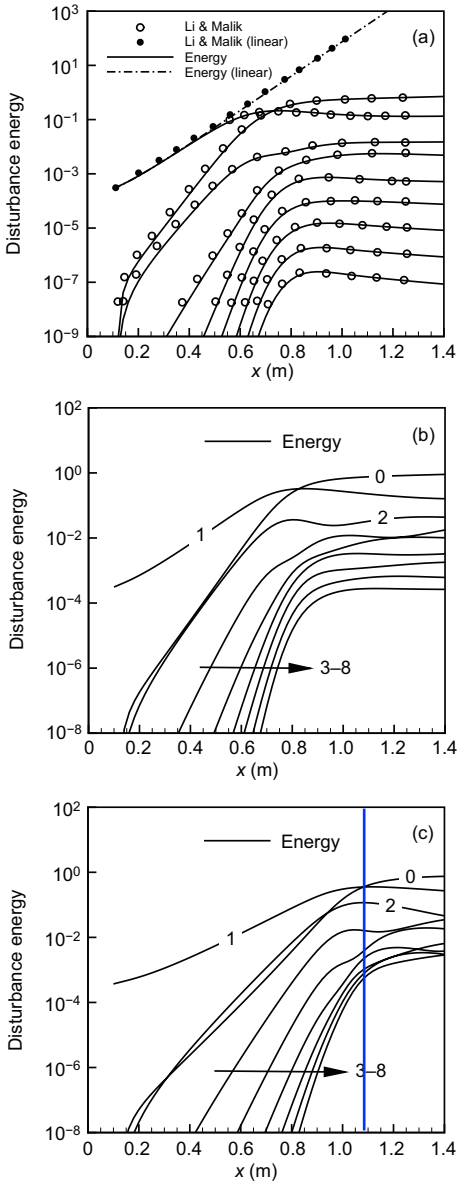

Figure 1 Disturbance energy of the nonlinear development of Görtler vortices with Fourier mode $(0,0)$ – $(0,8)$. (a) λ = 9 mm. The circles denote the results given by Li and Malik [1]; (b) λ = 18 mm; (c) λ = 36 mm.

the streamwise direction, equation (2) is thus simplified as

$$Q(y,z) = \bar{q}_0(y) + \sum_{n=-\infty}^{\infty} \bar{Q}_n(y)\, \mathrm{e}^{\mathrm{i}n\beta z}. \tag{13}$$

By substituting eqs. (12) and (13) into the N-S equations, the curvature-related terms are neglected due to the inviscid nature of the secondary instability. The eigenvalue problem is finally formulated as

$$\mathcal{L}\Theta = \sigma\mathcal{R}\Theta. \tag{14}$$

The system is discretized for numerical solutions. The Chebyshev collocation method (9) is also used here in the normalwise direction with N_y grid points. The Fourier collocation method in eq. (12) is used in the spanwise direction with N_z points due to its periodicity. As a result, $\mathcal{L}$ and $\mathcal{R}$ are sparse square matrix of size $\left(N_y \times N_z \times 5\right)^2$. The generalized eigenvalue problem is solved with the Arnoldi method.

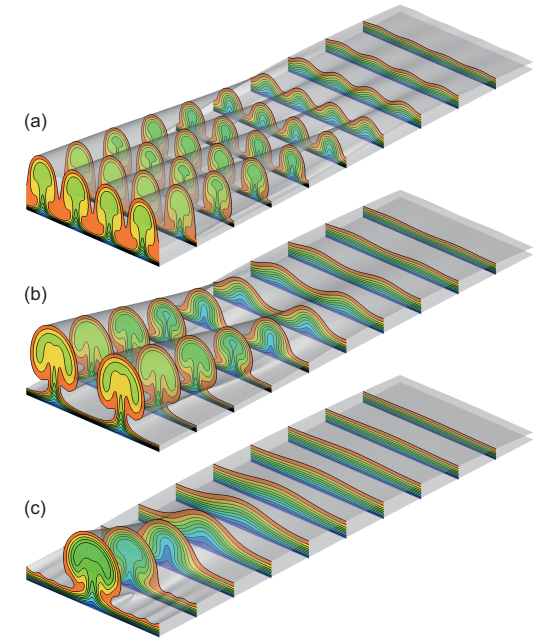

Figure 2 The nonlinear development of Görtler vortices characterized by the streamwise velocity, contour levels = 0.1 – 0.9. (a) λ = 9 mm; (b) λ = 18 mm; (c) λ = 36 mm.

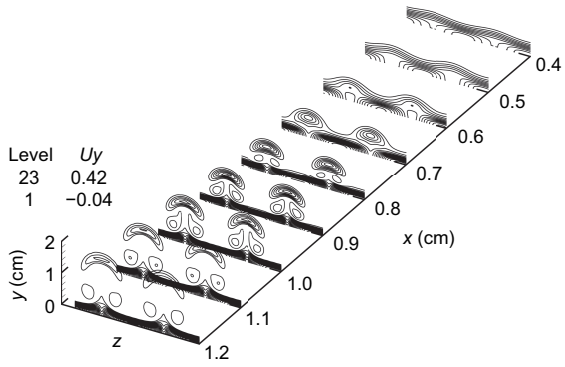

Figure 3 The normalwise gradient of the streamwise velocity $\frac{\partial U}{\partial y}$, λ = 18 mm.

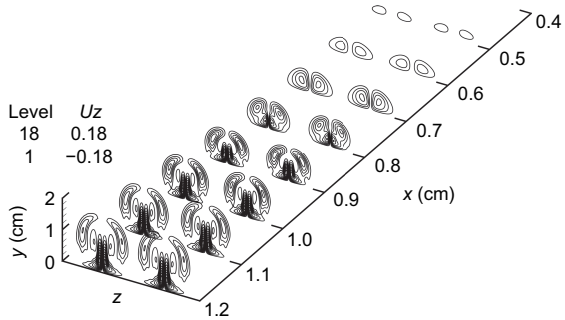

Figure 4 The spanwise gradient of the streamwise velocity $\frac{\partial U}{\partial z}$, λ = 18 mm.

4 Fundamental mode

The 18 mm-wavelength case is chosen for the analysis of the secondary instability. From the analysis of Li and Malik [1], it is shown that the growth rate of the secondary instability becomes larger as the Görtler vortices gather strength towards their saturation states. Back to the base flow shown in Figure 2, the saturation state is reached at about $x = 100$ cm. Here we give the results of three streamwise stations $x = 95, 100$ and 105 cm in Figure 5. The most amplified four modes are given. Through comparing the three stations, the growth rate of the most amplified mode within its wavenumber scope remains nearly unchanged but a slight drop at $x = 105$ cm. Thus it can be inferred that the growth rate of the secondary disturbances drops in the over-saturated Görtler vortices.

These modes are termed the even modes and odd modes according to the symmetry or dissymmetry of the eigenfunctions. For the 18 mm case, the most amplified mode is the even mode I. The largest growth rate is brought about by the corresponding wavenumber shown in Table 1. The most dangerous wavenumber lies between 0.21 and 0.27 corresponding to the wavelength of 1.27–1.64 cm except odd mode II. This is the length scale of the boundary layer thickness.

A special feature is shown by odd mode II. The growth rate of this mode exceeds the others in the large wavenumber regime, i.e. $\alpha_s > 0.38-0.39$ and odd mode II reaches its maximum at $\alpha_s = 0.47 - 0.48$. This wavenumber is nearly twice the most amplified wavenumber of the other modes thus the disturbances governed by odd mode II bear a smaller length scale in the streamwise direction.

Here we show the eigenfunctions of the four modes in Figure 6. The streamwise velocity component $|u_s|$ is plotted together with the corresponding base flow at $x = 95$ cm. Both the disturbances and the base flows are normalized so that they have the unity maximum value. The wavenumber α_s is specified as 0.225 (wavelength $\lambda_x = 1.53$ cm), thus the modes in descending order of the growth rate are even mode I, odd mode I, even mode II and odd mode II.

A comparison can be made here with the inviscid calculation by Li and Malik (pp.87, Figure 5) [1]. The overall shapes of the disturbances coincide with each other. A close look at odd mode I and even mode II shows the suppression of the disturbances near the wall. This distinction can be attributed to the inviscid equations used by Li and Malik [1]. The diffusion caused by the viscosity is therefore eliminated. In general, the secondary instability is inviscid in nature and the ignored viscosity should not create an essential influence.

Finally we focus on odd mode II which was not reported by Li and Malik (pp.85, Figure 3) [1]. The disturbances are concentrated near the stem of the mushroom near the wall. A global method which finds all the eigenvalues was used by them, thus the missing part should be for the inviscid analysis. The largest growth rate of this mode is yet less than that of even mode I. Within the cases studied here, odd

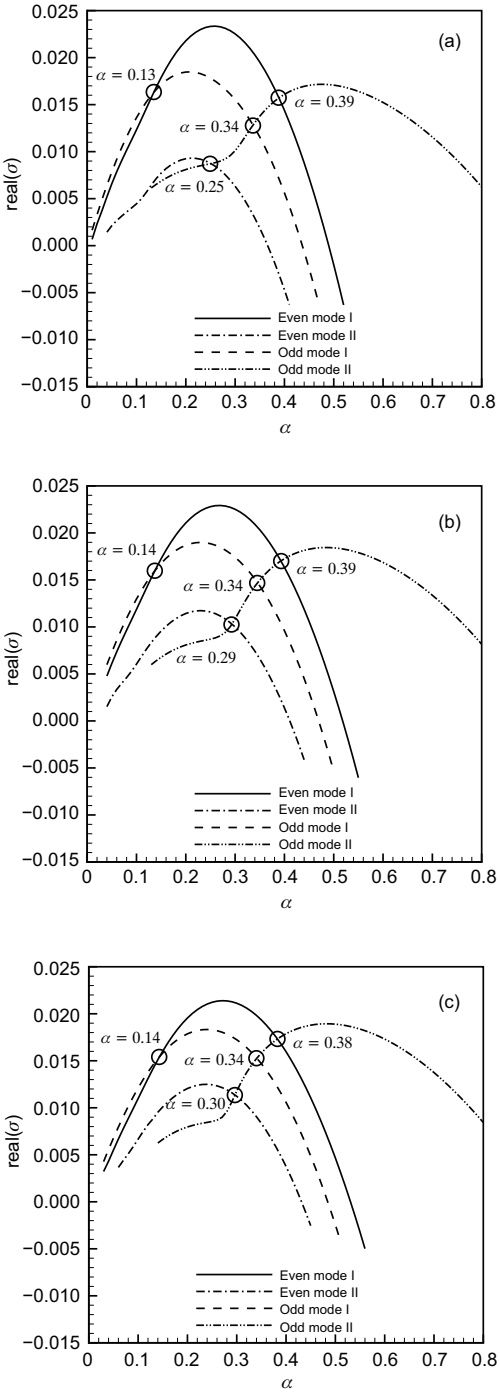

Figure 5 The growth rate of the secondary disturbances at (a) $x = 95$ cm; (b) $x = 100$ cm and (c) $x = 105$ cm. The most amplified four modes are shown.

Table 1 The wavenumber at which the four modes are most amplified

α_s	$x = 95$ cm	$x = 100$ cm	$x = 105$ cm
Even mode I	0.26	0.27	0.27
Even mode II	0.21	0.23	0.24
Odd mode I	0.21	0.23	0.24
Odd mode II	0.47	0.48	0.48

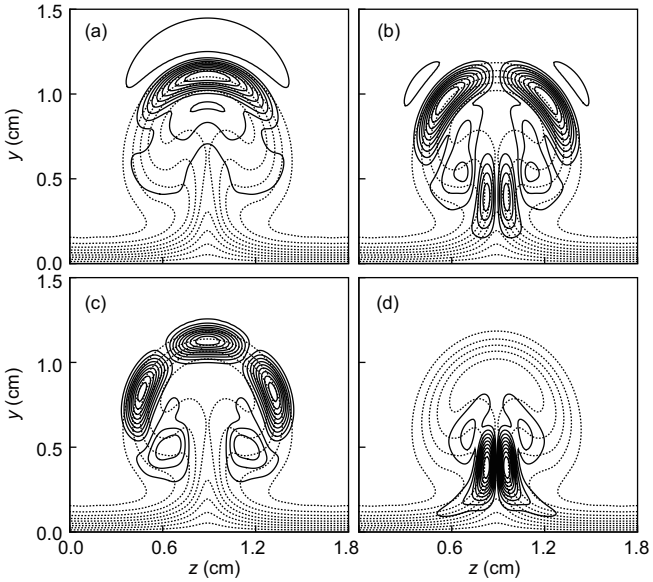

Figure 6 Contours of the secondary disturbances u (absolute value, solid lines) with the base flow (dashed lines). Nine levels are specified from 0.1 to 0.9. (a) Even mode I; (b) odd mode I; (c) even mode II; (d) odd mode II.

mode II should not appear in the experiment.

5 Subharmonic and detuned modes

In this section, the influence of Floquet parameter γ is studied. Here we introduce $\varepsilon = \gamma_i/\beta$ and thus $0 < \varepsilon < 0.5$ and $\varepsilon = 0.5$ give the detuned and subharmonic modes respectively. The influence of the Floquet parameter on the growth rate of the four modes is within 3.5% as shown in Figure 7.

The growth rates of the subharmonic modes are larger than their fundamental counterparts except odd mode I. According to the results of Li and Malik [1], even mode I is stronger for the large wavelengths while odd mode I is stronger for the small wavelengths. As a result, the even mode tends to appear as the subharmonic type while the odd mode tends to appear as the fundamental.

The Floquet parameter does not alter the absolute value of the disturbances but a phase change. The real parts of disturbances u are shown in Figure 8 for the subharmonic modes and Figure 9 for the detuned modes with a Floquet parameter of $\gamma_i = 0.25\beta$.

The subharmonic modes show a phase reverse. Both the subharmonic and detuned modes bear the spanwise wavelength twice that of the base flow. The detuned modes are rarely reported in the existing articles. In the current cases, they have the growth rates lower than the fundamental or subharmonic modes. Hence, no occurrence should be noticed in the experiments.

6 Concluding remarks

Secondary instability analysis is carried out for the classic experiment conducted by Swearingen and Blackwelder [9].

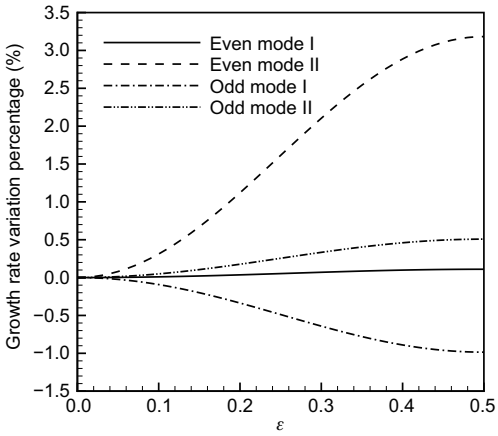

Figure 7 Influence of the Floquet parameter on the variation of growth rate of the four modes.

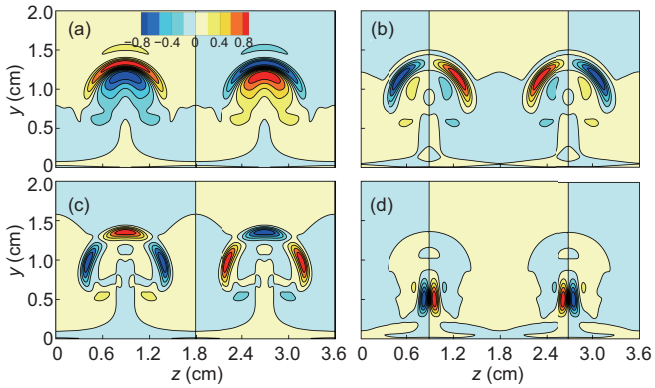

Figure 8 Contours of the secondary disturbances u (real part) for the subharmonic instability at $x = 105$ cm, $\alpha_s = 0.3$. (a) Even mode I; (b) odd mode I; (c) even mode II; (d) odd mode II.

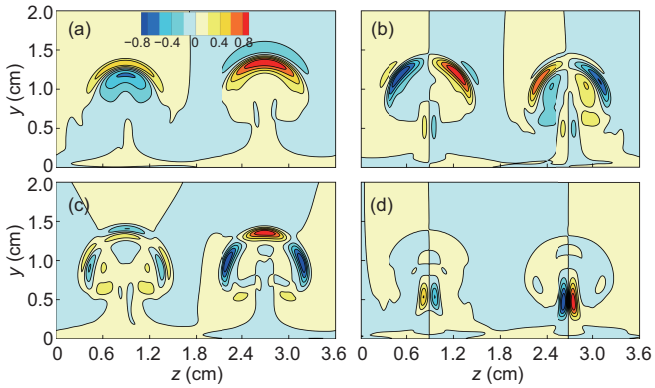

Figure 9 Contours of the secondary disturbances u (real part) for the detuned instability at $x = 105$ cm, $\alpha_s = 0.3$. (a) Even mode I; (b) odd mode I; (c) even mode II; (d) odd mode II.

The NPSE is formulated and numerically solved for the base flow. The saturated Görtler vortices considerably distort the Blasius boundary layer and are responsible for the secondary instabilities.

Floquet theory is applied in the formulation of the secondary instability. For the 18mm case of the base flow, fundamental modes are given for three streamwise stations near the saturation point. The most amplified four modes observed are even I, odd I, even II and odd II. The mode even I is the most amplified mode and will result in the horseshoe type breakdown. Odd mode II missing in Li and Malik's work [1] shows some unique features against the other three. The most dangerous streamwise wavenumber for this mode is nearly twice the others and it will dominate in a large wavenumber regime.

Together with the fundamental modes, the subharmonic and detuned counterparts also exist for each mode. The absolute values of the eigenfunctions of the three types are exactly identical but a phase change. The growth rate of the subharmonic mode even exceeds that of the fundamental mode except odd mode I. Therefore, it can be concluded that the subharmonic mode is responsible for the transition process. This is in correspondence with the observation of the experiment where the mushrooms are attracted or move away with each other.

Finally, it should be noted that the present study is limited to the incompressible flows with elaborate experiment available. Exploration into the supersonic and hypersonic flows, either experimentally or numerically, is still far from requirement.

The authors thank Dr. XU GuoLiang and Dr. LIU JianXin for valuable comments and suggestions. The work was supported by the National Natural Science Foundation of China (Grant Nos. 10932005 and 11202115).

1 Li F, Malik M R. Fundamental and subharmonic secondary instabilities of Görtler vortices. J Fluid Mech, 1995, 297: 77–100
2 Denier J P, Hall P, Seddougui S O. On the receptivity problem for Görtler vortices: Vortex motions induced by wall roughness. Philo Trans Royal Soc A, 1991, 335: 51–85
3 Herbert T. On the stability of the boundary layer along a concave wall. Archiwum Mechaniki Stosowanej, 1976, 28: 1039–1055
4 Hall P. Görtler vortices in growing boundary-layers: The leading-edge receptivity problem, linear growth and the nonlinear breakdown stage. Mathematika, 1990, 37: 151–189
5 Floryan J M. On the Görtler instability of boundary layers. Prog Aerosp Sci, 1991, 28: 235–271
6 Saric W S. Görtler vortices. Annu Rev Fluid Mech, 1994, 26: 379–409
7 Herbert T. Secondary instability of plane channel flow to subharmonic three-dimensional disturbances. Phy Fluids, 1983, 26: 871–874
8 Herbert T. Secondary instability of boundary layers. Annu Rev Fluid Mech, 1989, 20: 487–526
9 Swearingen J D, Blackwelder R F. The growth and breakdown of streamwise vortices in the presence of a wall. J Fluid Mech, 1987, 182: 255–290
10 Lee K, Liu J T C. On the growth of mushroomlike structures in nonlinear spatially developing Goertler vortex flow. Phys Fluids A, 1992, 4: 95–103
11 Hall P. The nonlinear development of Görtler vortices in growing boundary layers. J Fluid Mech, 1988, 193: 243–266
12 Hall P, Horseman N J. The linear inviscid secondary instability of longitudinal vortex structures in boundary layers. J Fluid Mech, 1991, 232: 357–375
13 Herbert T. Parabolized stability equations. Annu Rev Fluid Mech, 1997, 29: 245–283
14 Yu X, Liu J T C. On the mechanism of sinuous and varicose modes in three-dimensional viscous secondary instability of nonlinear Görtler rolls. Phys Fluids, 1994, 6: 736–750
15 Benmalek A, Saric W S. Effects of curvature variations on the nonlinear evolution of Görtler vortices. Phys Fluids, 1994, 6: 3353–3367
16 Cunff C L, Zebib A. Nonlinear spatially developing Görtler vortices in curved wall jet flow. Phys Fluids, 1996, 8: 2375–2384
17 Liu Y, Zaki T A, Durbin P A. Floquet analysis of secondary instability of boundary layers distorted by Klebanoff streaks and Tollmien-Schlichting waves. Phys Fluids, 2008, 20: 1–16
18 Wu X S, Zhao D F, Luo J S. Excitation of steady and unsteady Görtler vortices by free-stream vortical disturbances. J Fluid Mech, 2011, 682: 66–100
19 Schrader L U, Brandt L, Zaki T A. Receptivity, instability and breakdown of Görtler flow. J Fluid Mech, 2011, 682: 362–396
20 Xu G L, Xiao Z X, Fu S. Analysis of the secondary instability of the incompressible flows over a swept wing. Sci China-Phys Mech Astron, 2011, 54: 724–736
21 Xu G L, Xiao Z X, Fu S. Secondary instability control of compressible flow by suction for a swept wing. Sci China-Phys Mech Astron, 2011, 54: 2040–2052
22 Chang C L, Malik M R. Oblique-mode breakdown and secondary instability in supersonic boundary layers. J Fluid Mech, 1994, 273: 323–360
23 Schmid P J, Henningson D S. Stability and Transition in Shear Flows. New York: Springer-Verlag, 2001